

Fig. S1. Schematic figure to show the method for quantify the IHC results. A schematic figure to show the method for the IHC quantification. A) The area in CA1 and CA3 where the image (200X magnification) was taken was indicated by red frame. B) An example to show how the software works. Briefly, in each section, the subfield of interest (pyramidal layer) was manually (digitally) outlined as indicated in Fig. S1A, and its area was measured. A threshold was set and only the objects with a staining level above this threshold were measured (Fig. S1B). Staining intensity was measured in the fraction of subfield of region of interest (ROI) area occupied by the threshold object area (object area/ROI area) within the selected areas outlined by the drawing tool. (Colours are visible in the electronic version of the article at www.iospress.nl)

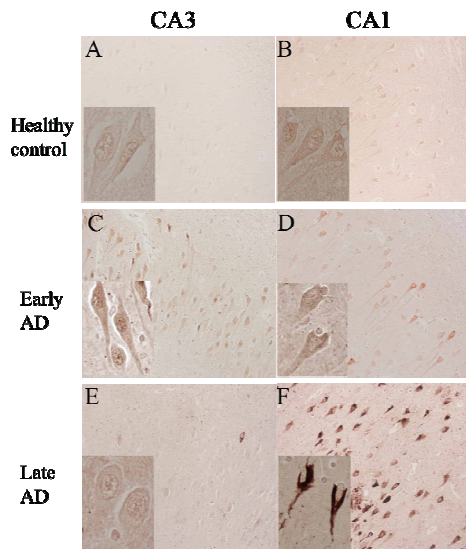


Fig. 4. The distribution of Abl-pT735 in control, early AD, and late AD hippocampus. Immunohistochemistry of Abl-pT735 in the CA3 (Left column) and CA1 (Right column) of healthy controls (A and B), early stage AD (C and D), and late stage AD (E and F). Magnification for all panels is 200X and inset magnification is 400X. (Colours are visible in the electronic version of the article at www.iospress.nl)

pus (Fig. 6A). *c-Abl* immunoreactivity increased in late AD but remained lower than control subjects (Fig. 6A). *c-Abl* levels in the CA3 exhibited a statistically significant decrease across all three subject groups (Fig. 6A). However levels of Abl-pY412 were significantly higher in the CA1 of early AD than control or late AD subjects (Fig. 6B). A similar trend was evident in the CA3 (Fig. 6B), suggesting the accumulation of Abl-pY412 during early AD. We observed increased Abl-pT735 immunoreactivity in the CA1 and CA3 of late AD when

compared to control and early AD, with statistically significant increase in CA1 (Fig. 6C).

Co-localization of activated c-Abl with hyperphosphorylated tau and amyloid plaques

We next examined the co-localization of phospho-*c-Abl* isoforms with hyperphosphorylated tau (p-tau) during AD by double-label laser confocal microscopy. Abl-pY412 co-localized with phosphorylated tau in GVDs within NFTs bearing neurons and co-localized within tau-positive granules in amyloid plaques in late AD (Fig. 7). Abl-pY412 and p-tau co-localized all Abl-pY412 immunopositive neurons. Abl-pT735 co-localized with p-tau in both GVDs and NFTs (Fig. 8, panels A-F). All Abl-pT735 positive neurons were p-tau positive, with all p-tau positive GVDs also immunoreactive for Abl-pT735. Punctate Abl-pT735 immunoreactivity was also observed within amyloid plaques (Fig. 8, panels G-I), although it was not co-localized with $A\beta$.

Finally, we co-immunoprecipitated *c-Abl* and p-tau from AD hippocampus (Fig. 9). Immunoprecipitation of *c-Abl* resulted in the co-precipitation of p-tau specifically in AD brain (Fig. 9A). We also observed co-immunoprecipitation of *c-Abl* by immunoprecipitation of p-tau from AD or control brain (Fig. 9B). These data suggest interactions between *c-Abl* and p-tau in the hippocampus.

In summary, we examined the expression and distribution of *c-Abl* in control and AD hippocampus. The highest level of *c-Abl* (unphosphorylated form) immunoreactivity was observed in healthy controls. Abl-pY412 exhibited abundant immunoreactivity dur-